

# Single-measurement digital optical frequency comb based phase-detection Brillouin optical time domain analyzer

CHAO JIN,<sup>1</sup> LIANG WANG,<sup>2,7</sup> YULI CHEN,<sup>3</sup> NAN GUO,<sup>1</sup> WENGHONG CHUNG,<sup>4</sup> HOYIN AU,<sup>4</sup> ZHAOHUI LI,<sup>5,6</sup> HWA-YAW TAM,<sup>4</sup> AND CHAO LU<sup>1</sup>

<sup>1</sup>Photonics Research Centre, The Hong Kong Polytechnic University, Hong Kong, China

<sup>2</sup>Department of Electronic Engineering, The Chinese University of Hong Kong, Shatin, N.T., Hong Kong, China

<sup>3</sup>Department of electronic engineering, Jinan University, Guangzhou 510632, China

<sup>4</sup>Photonics Research Center, Department of Electrical Engineering, The Hong Kong Polytechnic University, Kowloon, Hong Kong SAR, China

<sup>5</sup>State Key Laboratory of Optoelectronic Material and Technologies and School of Electronics and Information Technology, Sun Yat-sen University, Guangzhou 510632, China

<sup>6</sup>lzh88@sysu.edu.cn

<sup>7</sup>lwang@ee.cuhk.edu.hk

**Abstract:** A single-measurement sweep-free distributed Brillouin optical time domain analyzer (BOTDA) sensor based on phase detection is proposed and experimentally demonstrated employing digital optical frequency comb (DOFC) probe signal. Brillouin Phase Spectrum (BPS) of DOFC probe induced by Brillouin interaction is measured using coherent detection in a single acquisition, without any frequency scanning and data averaging. Single-measurement BOTDA sensor based on BPS in 10km long fiber is demonstrated with a response time of 100  $\mu$ s, which is limited only by the fiber length. The spatial resolution is 51.2m, determined by the duration of DOFC. And the Brillouin frequency shift (BFS) uncertainty is estimated to be  $\sim$ 1.5 MHz at the end of fiber under test (FUT). Benefiting from the fast response time, dynamic measurement up to 1 kHz vibration frequency has been demonstrated.

© 2017 Optical Society of America

**OCIS codes:** (060.2370) Fiber optics sensors;(290.5900) Scattering, stimulated Brillouin;(190.0190) Nonlinear optics.

## References and links

1. T. Horiguchi and M. Tateda, "Optical-fiber-attenuation investigation using stimulated Brillouin scattering between a pulse and a continuous wave," *Opt. Lett.* **14**(8), 408–410 (1989).
2. T. Horiguchi, T. Kurashima, and M. Tateda, "Tensile strain dependence of Brillouin frequency shift in silica optical fibers," *IEEE Photonics Technol. Lett.* **1**(5), 107–108 (1989).
3. R. Bernini, A. Minardo, and L. Zeni, "Dynamic strain measurement in optical fibers by stimulated Brillouin scattering," *Opt. Lett.* **34**(17), 2613–2615 (2009).
4. Y. Peled, A. Motil, L. Yaron, and M. Tur, "Slope-assisted fast distributed sensing in optical fibers with arbitrary Brillouin profile," *Opt. Express* **19**(21), 19845–19854 (2011).
5. Y. Peled, A. Motil, I. Kressel, and M. Tur, "Monitoring the propagation of mechanical waves using an optical fiber distributed and dynamic strain sensor based on BOTDA," *Opt. Express* **21**(9), 10697–10705 (2013).
6. Y. Peled, A. Motil, and M. Tur, "Fast Brillouin optical time domain analysis for dynamic sensing," *Opt. Express* **20**(8), 8584–8591 (2012).
7. X. Bao, C. Zhang, W. Li, M. Eisa, S. El-Gamal, and B. Benmokrane, "Monitoring the distributed impact wave on a concrete slab due to the traffic based on polarization dependence on stimulated Brillouin scattering," *Smart Mater. Struct.* **17**(1), 015003 (2008).
8. A. Voskoboinik, J. Wang, B. Shamee, S. R. Nuccio, L. Zhang, M. Chitgarha, A. E. Willner, and M. Tur, "SBS-Based Fiber Optical Sensing Using Frequency-Domain Simultaneous Tone Interrogation," *J. Lightwave Technol.* **29**(11), 1729–1735 (2011).
9. A. Voskoboinik, O. F. Yilmaz, A. W. Willner, and M. Tur, "Sweep-free distributed Brillouin time-domain analyzer (SF-BOTDA)," *Opt. Express* **19**(26), B842–B847 (2011).

10. A. Voskoboinik, D. Rogawski, H. Huang, Y. Peled, A. E. Willner, and M. Tur, "Frequency-domain analysis of dynamically applied strain using sweep-free Brillouin time-domain analyzer and sloped-assisted FBG sensing," *Opt. Express* **20**(26), B581–B586 (2012).
11. I. Sovran, A. Motil, and M. Tur, "Frequency-scanning BOTDA with ultimately fast acquisition speed," *IEEE Photonics Technol. Lett.* **27**(13), 1426–1429 (2015).
12. Y. Mizuno, N. Hayashi, H. Fukuda, K. Y. Song, and K. Nakamura, "Ultra high speed distributed Brillouin reflectometry," *Light Sci. Appl.* **5**(12), e16184 (2016).
13. E. Preter, D. Ba, Y. London, O. Shlomi, Y. Antman, and A. Zadok, "High-resolution Brillouin optical correlation domain analysis with no spectral scanning," *Opt. Express* **24**(24), 27253–27267 (2016).
14. J. Fang, W. Shieh, and P. Xu, "Single-shot Brillouin optical time domain analysis for distributed fiber sensing," in *Proceedings of IEEE Conference on Sensors* (2016), pp. 1–3.
15. X. Bao and L. Chen, "Recent progress in optical fiber sensors based on Brillouin scattering at university of Ottawa," *Photon. Sensors* **1**(2), 102–117 (2011).
16. T. Sperber, A. Eyal, M. Tur, and L. Thévenaz, "High spatial resolution distributed sensing in optical fibers by Brillouin gain-profile tracing," *Opt. Express* **18**(8), 8671–8679 (2010).
17. M. A. Soto, G. Bolognini, and F. Di Pasquale, "Optimization of long-range BOTDA sensors with high resolution using first-order bi-directional Raman amplification," *Opt. Express* **19**(5), 4444–4457 (2011).
18. C. Jin, N. Guo, Y. Feng, L. Wang, H. Liang, J. Li, Z. Li, C. Yu, and C. Lu, "Scanning-free BOTDA based on ultra-fine digital optical frequency comb," *Opt. Express* **23**(4), 5277–5284 (2015).
19. X. Tu, Q. Sun, W. Chen, M. Chen, and Z. Meng, "Vector Brillouin optical time-domain analysis with heterodyne detection and IQ demodulation algorithm," *IEEE Photonics J.* **6**(2), 1–8 (2014).
20. X. Angulo-Vinuesa, A. Lopez-Gil, A. Dominguez-Lopez, J. L. Cruz, M. V. Andres, S. Martin-Lopez, and M. Gonzalez-Herraez, "Simultaneous gain and phase profile determination on an interferometric BOTDA," *Proc. SPIE* **9634**, 963419 (2015).
21. Z. Li, L. Yan, L. Shao, W. Pan, and B. Luo, "Coherent BOTDA sensor with intensity modulated local light and IQ demodulation," *Opt. Express* **23**(12), 16407–16415 (2015).
22. A. Lopez-Gil, X. Angulo-Vinuesa, M. A. Soto, A. Dominguez-Lopez, S. Martin-Lopez, L. Thévenaz, and M. Gonzalez-Herraez, "Gain vs phase in BOTDA setups," *Proc. SPIE* **9916**, 991631 (2016).
23. A. Lopez-Gil, M. A. Soto, X. Angulo-Vinuesa, A. Dominguez-Lopez, S. Martin-Lopez, L. Thévenaz, and M. Gonzalez-Herraez, "Evaluation of the accuracy of BOTDA systems based on the phase spectral response," *Opt. Express* **24**(15), 17200–17214 (2016).
24. J. Urricelqui, A. Zornoza, M. Sagues, and A. Loayssa, "Dynamic BOTDA measurements based on Brillouin phase-shift and RF demodulation," *Opt. Express* **20**(24), 26942–26949 (2012).
25. S. Díaz, S. M. Foaleng, M. López-Amo, and L. Thévenaz, "High performance Brillouin distributed fibre sensor," *Proc. SPIE* **6619**, 661938 (2007).
26. J. Yang, C. Yu, Z. Chen, J. Ng, and X. Yang, "Suppression of polarization sensitivity in BOTDA fiber distributed sensing system," *Proc. SPIE* **7004**, 700421 (2008).
27. J. Urricelqui, F. López-Fernandino, M. Sagues, and A. Loayssa, "Polarization diversity for Brillouin distributed fiber sensors based on a double orthogonal pump," *Proc. SPIE* **9157**, 91576A (2014).
28. J. Urricelqui, F. López-Fernandino, M. Sagues, and A. Loayssa, "Polarization diversity scheme for BOTDA sensors based on a double orthogonal pump interaction," *J. Lightwave Technol.* **33**(12), 2633–2638 (2015).
29. W. Shieh, H. Bao, and Y. Tang, "Coherent optical OFDM: theory and design," *Opt. Express* **16**(2), 841–859 (2008).
30. E. Ip, A. P. T. Lau, D. J. F. Barros, and J. M. Kahn, "Coherent detection in optical fiber systems," *Opt. Express* **16**(2), 753–791 (2008).
31. K. M. Wolter, *introduction to variance estimation* (Springer Science + Business Media, 2007), Chap. 6.
32. Z. Songlin and Z. Kun, "Approximate computation of expectation and variance of nonlinear function of continuous random variable," *J. Geodesy. Geodyn.* **28**, 107 (2008).

## 1. Introduction

Distributed Brillouin optical time domain analyzer (BOTDA) has been intensively investigated in recent decades. The capability to provide highly precise and distributed measurements of strain and temperature profile has been demonstrated [1, 2]. A wide variety of applications including border security, temperature analysis and structure health monitoring have been studied extensively. One major limitation for BOTDA is the slow response speed. Intensive research has been devoted to improve the measurement speed of Brillouin based sensor [3–14]. To operate the distributed optical fiber sensors in dynamic mode would be of great importance in many application fields, such as measurement of vibrations in civil or aeronautic structures which requires a monitoring speed in the range of seconds or even less.

There are two major factors limiting the speed of a BOTDA. One is the scanning of probe or pump frequency and the other is large amount of averaging times due to poor signal-to-noise ratio (SNR).

The first issue means that it is necessary to scan the whole Brillouin Gain Spectrum (BGS) to identify the Brillouin frequency shift (BFS). Typically, in conventional BOTDA, the probe or pump signal need to be swept in frequency domain more than 100 times around the BFS to interrogate Brillouin amplification characteristics at different positions along the fiber [15–17], which severely limits the demodulation speed of the BFS distribution along the optical fiber. Several novel BOTDA techniques have been proposed to achieve fast and dynamic sensing, including slope-assisted BOTDA [3–5], sweep-free BOTDA [8–10] and ultra-fast sweeping scheme [11,12]. Moreover, we have recently proposed a digital optical frequency comb (DOFC) based scanning-free BOTDA system to facilitate the flexible reconstruction process of BGS without any frequency scanning [18].

However, all of these schemes are based on direct detection of the probe signal intensity. Due to the poor SNR, beyond hundreds of averaging times is inevitable to enhance the measurement precision. While, phase detection has been considered as a promising candidate since Brillouin phase shift spectrum in the vicinity of BFS has been proved to be quasi-linear, which is far more sensitive than the intensity variation near the Brillouin gain peak. Several techniques have been proposed to characterize the Brillouin Phase Spectrum (BPS) [19–21], and the benefits of BPS when used to determine BFS has been demonstrated in [22, 23]. The high sensitivity of BPS has been applied in dynamic strain measurement with the advantage of large tolerance to variations in fiber attenuation or changes in pump pulse power [24].

In this work, we report a single-measurement BOTDA based on coherent detection of the phase of DOFC probe signal without any averaging and frequency scanning process. The phase shift of each frequency component of DOFC probe, after transmitting through the fiber under test (FUT) is directly mapped by coherent demodulation in a single data acquisition without any averaging, leading to a sensing speed only limited by the sensing range. Compared with the previous technique in [18], the measurement time is further reduced by eliminating the need for averaging. And BPS detection instead of BGS has been performed for better accuracy. The performance of our scheme is analyzed through simulation and experiment. Distributed temperature sensing over 10km FUT has been demonstrated by using the proposed single-measurement BOTDA with a BFS uncertainty of 1.5 MHz and spatial resolution of 51.2 m. With the advantage of high speed, dynamic measurement up to 1 kHz vibration frequency has been demonstrated.

## 2. Sensing principle, generation and demodulation of digital electrical frequency comb

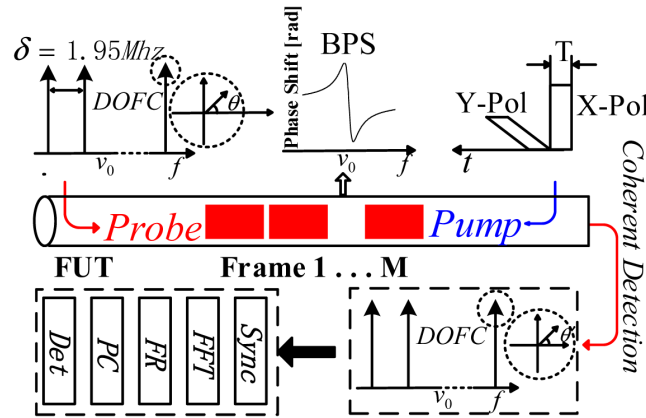


Fig. 1. Proposed BPS based BOTDA sensor scheme. DOFC: digital optical frequency comb; BPS: Brillouin phase spectrum; FUT: fiber under test; Sync: synchronization; FFT: Fast Fourier Transform; FR: frequency offset recovery; PC: phase noise compensation; Det: detection;  $\theta$ : pre-defined phase vector of the DOFC;  $\theta'$ : detected phase vector after Brillouin interaction in the FUT.

Fig. 1 presents the principle of the proposed scheme. In our scheme, the generation process of DOFC is quite similar to the one elaborated in [18], except that the pulse train of data used to generate digital electrical frequency comb (DEFC) is replaced by a complex signal with predefined phase offset vector  $\theta$ . The optical frequency comb is generated using Electro-Optic Modulator (EOM) driven by DEFC. In this way, the same initial phase offset of each DOFC frame is guaranteed. Note that tradeoff exists between spatial resolution and frequency spacing of DOFC. Higher spatial resolution results in worse frequency resolution and vice versa. The optical field for the transmitted DOFC probe signal could be expressed as:

$$E_s = \sum_{k=-\frac{N}{2}}^{\frac{N}{2}-1} e^{j(2\pi v_k t + \theta_k)}, v_k = k\delta \quad (1)$$

where  $N$  is the number of frequency tones and  $\delta$  is the frequency spacing between each tone.  $N$  frequency tones distributed symmetrically around probe wave are transmitted simultaneously with a spacing of  $\delta$ , resulting a sensing coverage range of  $N\delta$ . Orthogonally polarized pump pulses are utilized to excite Brillouin effect in the FUT, which can significantly eliminate the detrimental effects from polarization noise [25–28].

After Brillouin interaction with pump signal in FUT, the optical field of DOFC probe (normalized fields are assumed for simplicity) detected at coherent receiver is given by the following expression:

$$E_s = \sum_{k=-\frac{N}{2}}^{\frac{N}{2}-1} e^{j(2\pi v_k t + \theta_k)} H_{SBS}(v_k) \quad (2)$$

$H_{SBS}(v)$  is the complex Brillouin response spectrum for different frequency offset, which has the following form:

$$H_{SBS}(v) = (1 + g_v) e^{j\phi_v} \quad (3)$$

where  $g_v$  and  $\varphi_v$  are the Brillouin gain and phase spectrum, respectively. Then the phase shift  $\varphi$  recorded on each frequency component is retrieved by offline digital signal processing (DSP).

The post-processing algorithm has been investigated and used in coherent orthogonal frequency division multiplexing (OFDM) [29,30] communication systems to analyze and compensate fiber impairment during transmission. As the transmitted DOFC signal is known, the processing algorithm is simplified considerably and it is modified to best suit the sensing purpose. The proposed demodulation algorithm includes five parts, i.e. synchronization, Fast Fourier Transform (FFT), probe and local oscillator (LO) frequency offset recovery, phase noise compensation and detection. In the synchronization, we locate the temporal relationship of each detected DOFC frame by calculating the correlation between received frames and transmitted ones. In this way, the correlation peak and hence the temporal duration for each DOFC frame are readily determined. FFT is used subsequently to get the complex signal of each frequency tone and the angle of the complex signal is then calculated. By comparing the angle of the received complex signal with that of the transmitted one, the phase shift spectrum is easily obtained. As the phase shift is affected by the frequency offset and phase fluctuation between the probe and LO exist during coherent detection, frequency offset recovery and phase noise compensation is required to minimize the phase noise. Beating frequency between the probe and LO will inevitably lead to a continuous phase change of probe signal. Therefore, frequency offset is treated as the constant relative phase rotation between each DOFC frame and extra phase drift of adjacent frame due to frequency offset is calculated sequentially using the frequency offset recovery algorithm. To compensate the extra phase shift due to phase noise between LO and probe, here one of frequency tones (usually the first tone is used for convenience) is selected to serve as an accurate reference of phase fluctuation distribution and used for further compensation of the residual phase noise for the remaining frequency components. After the extra phase shift due to frequency offset and phase noise is compensated, the frequency-dependent Brillouin phase shift is simply obtained and BPS can be reconstructed accordingly. The BFS distribution as well as the temperature or strain along the fiber are obtained based on the measured BPS.

The determination of spatial resolution and location is the same as that in [18]. Unlike conventional BOTDA, the spatial resolution in our scheme is determined by the duration of DOFC frame. Probe signal is continuous but composed of  $M$  consecutive DOFC frames (indicated as frame 1 to  $M$ ) with minor time spacing between each other. In addition,  $M$  consecutive DOFC frames serve as probe to interact with pump in sequence through SBS in the fiber. In this way, FUT can be divided as  $M$  independent sections. The amplification and phase shift spectrum of individual interaction section is recorded by each DOFC frame. Hence, the minimum detectable length of fiber, namely the spatial resolution, is limited by the duration of DOFC frame (512 ns), resulting in a spatial resolution of 51.2 m in our case.

It should be noted that, recovered phase shift spectrum still suffers from the random intensity noise which is demonstrated in the following. The variance of the Gaussian noise affecting BGS and BPS is the same when using the interference method described in [22, 23], as the intensity variation is directly translated to the phase fluctuation. In our proposed method, the BPS is fully retrieved by coherent detection, and hence it results in an improved performance of phase noise variance. As described in the Appendix, the variance of phase noise can be expressed as follows:

$$D(\varphi_k) = \frac{\sigma^2/2}{1+g^2} \quad (4)$$

where  $\sigma$  is the stand deviation of measurement noise in Brillouin gain spectrum and  $g$  is the Brillouin gain coefficient. Note that the variance of phase noise in Eq. (4) is half of the

intensity noise. It implies that with the same obtained SNR, the averaging time can be reduced by 2 times. Simulations have been conducted to validate these expressions. Perfect BGS and BPS profile is assumed in the simulation. As in conventional BOTDA, SNR is defined as the inverse of maximum gain of time trace, which in this case equals to  $\frac{g}{\sigma}$ . In the simulation, 60 frequency tones with 2 MHz frequency spacing are utilized as DOFC probe signal. It should be noted that the intensity of complex optical field for each frequency tone is normalized. Figure 2 (a) shows the variance of phase noise and intensity noise as a function of SNR. It shows that the variance of phase noise is only half of the variance of intensity noise under the same SNR. Furthermore, the BFS error based on BGS and BPS are calculated and illustrated in Fig. 2 (b). 100 measurements are simulated to calculate the uncertainty of BFS. Lorentzian curve fitting (LCF) method is used for the determination of BFS based on BGS while linear fitting method is used for the case of BPS. Though both uncertainties using BGS and BPS deteriorate with the degradation of signal quality, the normalized uncertainty based on BPS still shows clear improvement under the worst situation where SNR is merely 6dB.

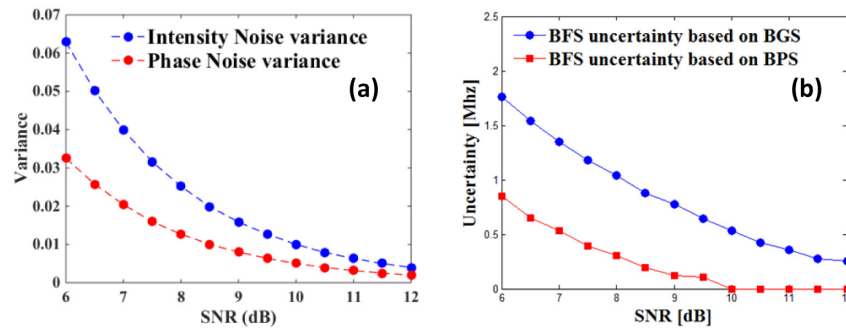


Fig. 2. (a) intensity noise variance and phase noise variance as a function of SNR. (b) BFS uncertainty based on BGS and BPS as a function of SNR.

### 3. Experiment setup

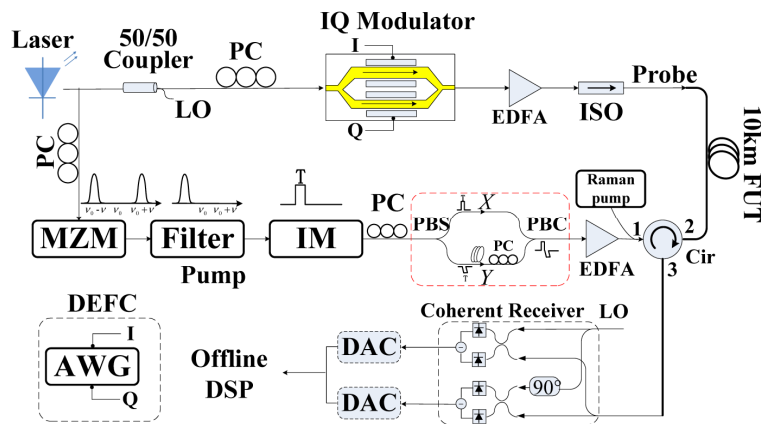


Fig. 3. Experiment setup of scanning-free BOTDA based on polarization-diversity pump. PC: polarization controller; EDFA: erbium-doped fiber amplifier; ISO: isolator; MZM: Mach-Zehnder modulator; IM: intensity modulator; PBS: polarizing beam splitter; PBC: polarizing beam combiner; Cir: circulator; LO: local oscillator; DAQ: data acquisition card; OSC: oscilloscope.

The experimental setup illustrated in Fig. 3 is used to achieve the proposed single-measurement BOTDA. A tunable laser operating at 1550 nm with 100 kHz linewidth is split into two parts by 3dB coupler to serve as pump and probe signal respectively.

Unlike the conventional implementation for frequency-sweep BOTDA, optical pump frequency is up-converted by modulation. A polarization controller (PC) is inserted between coupler and Mach-Zehnder modulator (MZM) to maintain high modulation efficiency. MZM biased at null point is driven by a synthesizer running at the frequency around the BFS to create the required sidebands. The maximum achieved extinction ratio of carrier suppression exceeds 30 dB. Then the higher frequency sideband is selected by a narrow bandwidth Fiber Bragg grating (FBG) filter before chopped by another intensity modulator (IM). Optical pulse series is generated through the IM driven by pulse generator which provides 100 ns long pulses with 8.3 kHz repetition rate. The IM allows shaping high extinction ratio optical pulses (~40 dB). The generated optical pulse series is then split by polarizing beam splitter (PBS) to two identical portions with orthogonal polarization state. A PC is inserted in front of PBS to adjust the state of polarization (SOP) of input pump signal and guarantee identical power in two polarization state. Another PC has been used in one of the branches in PBS/PBC structure in order to control SOP of the branch for polarization multiplexing. Before recombined in the subsequent polarizing beam combiner (PBC), one channel is delayed by a 20m single mode fiber (SMF) corresponding to the pulse width of 100 ns. The polarization multiplexed pump pair is directed into the FUT via a circulator after amplified by an erbium-doped fiber amplifier (EDFA). The average power of pump is set at 0 dBm. A Raman pump with a total power of ~200mW is co-propagating with Brillouin pump signal to compensate energy loss during transmission.

In the opposite direction, another 3dB coupler is used to divide the optical wave into two branches for probe optical signal and LO, respectively. It should be noted that the LO and probe signal are derived from the same laser source, which avoids significant laser frequency drift. More complicated frequency offset estimation and phase noise compensation algorithm are necessary if independent probe and LO laser is used. Probe signal is modulated by an IQ modulator with in phase and quadrature port driven by two independent channels of arbitrary waveform generator (AWG). The modulator output comprises a baseband optical frequency comb with a frequency range of 1 GHz and 1.95 MHz spacing. The optical power of the probe is set at 3dBm by EDFA before delivering it into the FUT where it counter-propagates with the pump signal to characterize the phase spectrum profile.

Integrated digital coherent receiver (ICR, Fujitsu FIM24704) is used at the receiver side to obtain the phase shift directly. After Brillouin frequency selective amplification, the probe signal from the FUT is delivered to the optical coherent receiver. Note that no extra EDFA is needed to compensate the energy loss of probe signal and satisfy the threshold of direct detection, which helps to eliminate the broadband noise induced by amplification. Probe signal is beating with LO and detected by balanced detector. The resultant electrical signals are collected by data acquisition card (DAQ) with 2 GHz sampling rate and further processed to obtain the distribution of BFS along the fiber.

#### 4. Measurement results

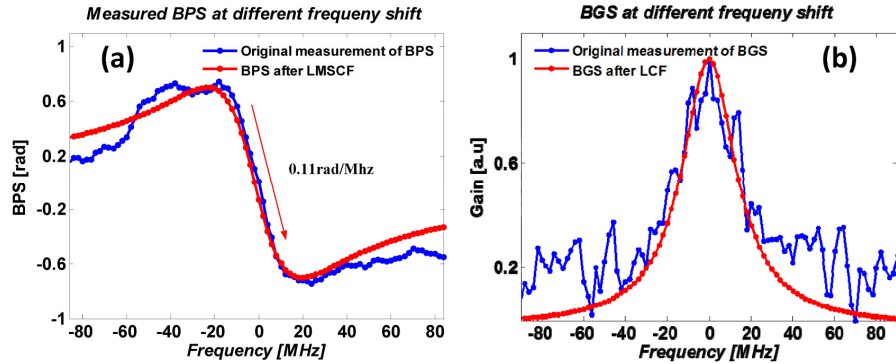


Fig. 4. Brillouin phase spectrum and Brillouin gain spectrum measured by the multi-tone probe signals at the beginning of FUT.

The sensing performance is evaluated using 10km SMF (composed of two 5km fiber reels) with uniform BFS distribution of 10.83GHz at room temperature (@1550nm). It should be noted that the calibration process is necessary to eliminate the distortions from electronic amplifier, photo-detector and environment variations. This can be done by recording the frequency response (including gain and phase characterization) of the multi-tone probe signals with a frequency granularity of 1.95MHz. The measured BPS without any applied environmental variance is shown in Fig. 4(a). The linear part of the BPS is about 40 MHz, equal to the linewidth of BGS. And the slope for the linear part is estimated to be 0.11 rad/MHz using least mean square curving fitting (LMSCF). The BFS is readily extracted by locating the linear center of BPS fitting process, which locates the characteristics of linear drop in the curve. Since BGS is simultaneously obtained in our configuration, we also show the results for BGS measurement. Original BGS is illustrated as the blue curve in Fig. 4 (b), while the BGS after LCF is shown as a red curve, with the estimated Full Width at Half Maximum (FWHM) of ~40MHz.

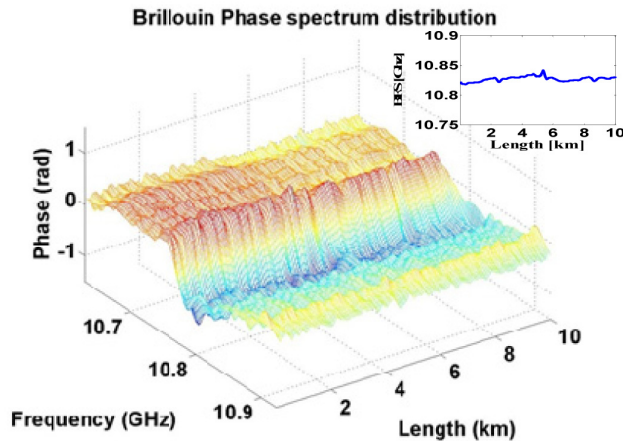


Fig. 5. Brillouin phase spectrum and the measured BFS distribution (inset) along the FUT.

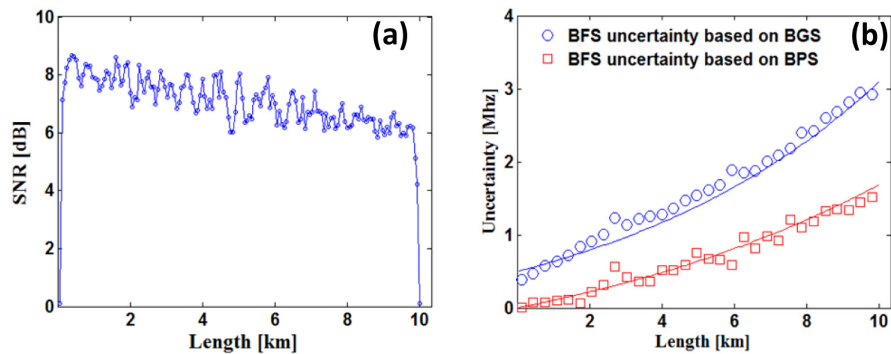


Fig. 6. (a) The SNR along FUT, defined by the maximum gain in the central of BGS normalized against noise deviation. No averaging is used in the measurement of SNR. (b) BFS uncertainty against distance calculated using BGS and BPS, respectively.

Then the BPS distribution along the FUT is analyzed and depicted in Fig. 5. As the Brillouin phase profile can be reconstructed without frequency scanning process and averaging, the resultant response speed of our proposed sensor is solely limited by the FUT length which is 10km in the experiment, corresponding to  $100 \mu s$ . The inset illustrates the corresponding BFS distribution extracted from the BPS. Assisted by the Raman amplification, the pump power depletion can be largely compensated and hence it maintains a power level to secure sufficient gain for the proposed scheme. The SNR and BFS uncertainty along FUT using are given in Fig. 6. Relatively poor SNR is observed due to the fact that no averaging is used in the experiment. Linear fitting method is used for the determination of BFS from BPS, while as a comparison LCF method is used to obtain BFS from BGS. BFS uncertainty is calculated by taking the standard deviation of 100 experimental measurement results. Though both uncertainties based on BPS and BGS deteriorate with the degradation of signal quality, the one using BPS is estimated to be  $\sim 1.5$  MHz at the end of FUT which is less than half of that for BGS. The mismatch of the absolute uncertainty value between Fig. 6 (b) and Fig. 2 (b) simulation result could be attributed to the polarization misalignment during the splitting and recombination of pump pulses and the imperfect orthogonality of pump pairs during propagation inside fiber.

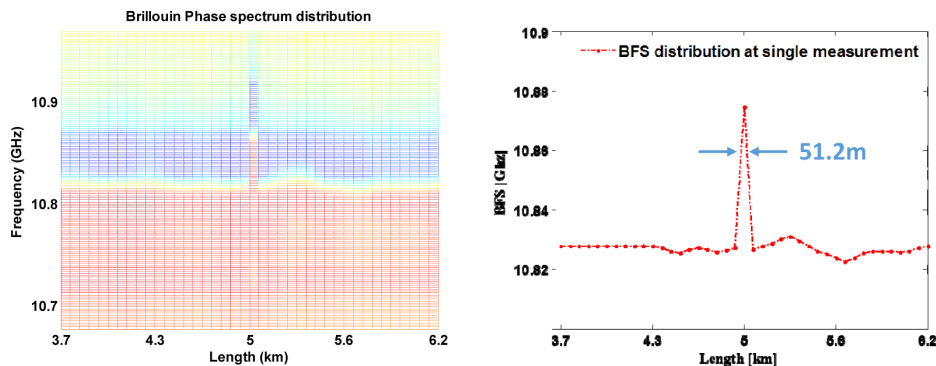


Fig. 7. Evaluation of spatial resolution with  $\sim 51$ m fiber section at the middle heated to  $60^\circ\text{C}$  (equivalent to 50MHz). (a) BPS distribution (b) BFS distribution.

In order to experimentally evaluate the spatial resolution of our scheme, 51-meter fiber section at the middle of FUT is heated by thermal chamber. Spatial resolution is determined through the measured BFS transition between the heated and unheated fiber sections. As shown in Fig. 7, the BPS and resultant BFS at the hot-spot section with a temperature of  $60^\circ\text{C}$  is different from those of section at room temperature, and the spatial resolution is found

to be 51.2 m at the temperature transition section, which matches well with 512-ns duration of the DOFC.

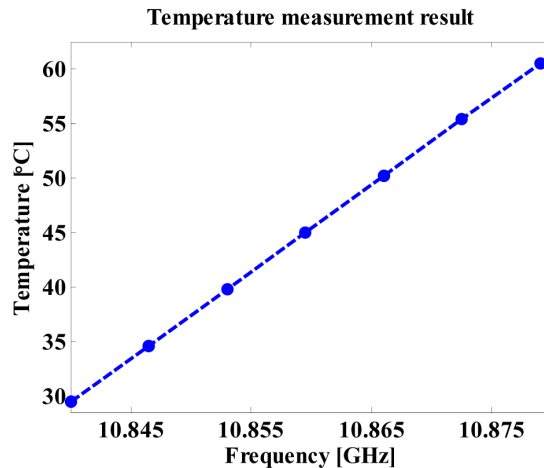


Fig. 8. Linear fitting results of temperature measurement.

To evaluate the temperature accuracy based on our scheme for BPS measurement, we heat the last 51m fiber of FUT from 30°C to 60°C with 5°C step. The measured BFS change with the temperature variation is depicted in Fig. 8. Maximum temperature measurement deviation from the linear fitting is about 0.5°C and temperature coefficient for this fiber is calculated to be 1.25 MHz/°C.

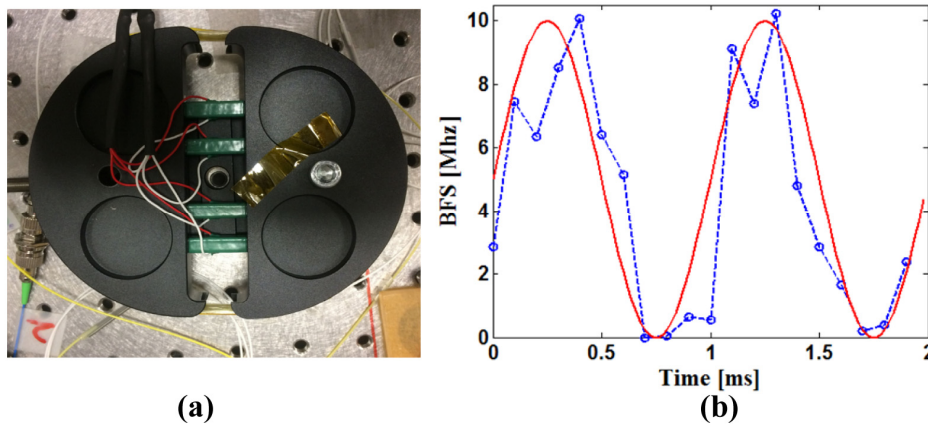


Fig. 9. Vibration measurement result. (a): Piezo-ceramic Transducers (PZT) fiber stretcher. (b): measured BFS variation as a function of time. Dynamic strain is applied by Piezo-ceramic Transducers (PZT) fiber stretcher with 51meter fiber wound on the PZT disk. The stretcher is driven by 1 kHz sinusoidal signal.

Moreover, vibration measurement using DOFC based phase-detection BOTDA has been demonstrated using PZT driven by 1 kHz sinusoidal signal. The strain coefficient of the fiber measured in the experiment is about 0.045 MHz/ $\mu\epsilon$  [18]. Thus, the theoretical dynamic range of strain is about 22500 $\mu\epsilon$ . Since our spatial resolution is 51.2m, 51m fiber is wound on the PZT for the demonstration of dynamic measurement. The results are given in Fig. 9. The time interval between each data point in Fig. 9 (b) is 0.1ms corresponding to a sampling rate of 10 kHz which is limited only by the fiber length (10km in our case). As shown in Fig. 9 (b) the BFS is measured to have a variation rate of 1 kHz, which confirms with the vibration

frequency applied on the 51m fiber. This indicates the successful measurement of dynamic strain using our scheme. Note that due to the limited elongation length of our PZT, the maximum BFS change is only 10MHz. Furthermore, non-uniform strain distribution on the 51m fiber induced by the imperfect winding process on the PZT distorts the BFS waveform from an ideal sinusoidal signal. All of these results in the discrepancy between the measurement result waveform and the applied vibration signal.

## 5. Conclusion

In summary, a single-measurement BOTDA sensor is proposed and experimentally demonstrated with 51 m spatial resolution over 10km fiber by employing coherent detection of BPS without any frequency scanning and averaging processes. The phase shift for all the frequency tones induced by Brillouin interaction are obtained in a single data acquisition. The response time of 100  $\mu$ s is limited only by the fiber length in our single-measurement BOTDA. Temperature measurement of 51m heated fiber over 10km FUT indicates a BFS uncertainty of 1.5 MHz and maximum temperature measurement deviation of 0.5°C. Dynamic measurement up to 1 kHz vibration frequency is successfully demonstrated to verify the dynamic characteristic of proposed technique. The high measurement speed and phase detection make the single-measurement BOTDA promising candidate for wide range of fast sensing scenarios with acceptable accuracy.

## Appendix

In the appendix, the variance of phase noise expressed in Eq. (4) is derived. Considering additive white Gaussian noise, the retrieved DOFC signal with described DSP method can be expressed as:

$$E_s = \sum_{k=-\frac{N}{2}-1}^{\frac{N}{2}} (1 + g_{v_k}) e^{j(\varphi_k)} \sigma \quad (5)$$

where  $\sigma$  is the stand deviation of measurement noise in Brillouin gain spectrum. The phase profile recovered from the DOFC signal is also distorted by random noise, as shown in the following equation:

$$\varphi_k = \text{Arg} \left[ (1 + g_{v_k}) e^{j(\varphi_k)} + \sigma \right] \quad (6)$$

for convenience, let:

$$I = (1 + g_{v_k}) e^{j(\varphi_k)} + \sigma \quad (7)$$

$$R = \frac{I_Q}{I_I} = \frac{\text{Im}[I]}{\text{Re}[I]} = \frac{(1 + g_{v_k}) \sin(\varphi_k)}{(1 + g_{v_k}) \cos(\varphi_k)}, \sigma = \sigma_I + j\sigma_Q \quad (8)$$

the unbiased estimation of  $R$  is:

$$\bar{R} = \tan(\varphi_k) \quad (9)$$

while the variance of  $R$  is given in [31]:

$$D(R) = \bar{R}^2 \left[ \frac{D(I_I)}{I_I^2} + \frac{D(I_Q)}{I_Q^2} - 2 \frac{c(I_I, I_Q)}{I_I I_Q} \right] \quad (10)$$

where  $I_I, I_Q$  represent for the In-phase and Quadrature component of  $I, D(I_I), D(I_Q)$ , and  $c(I_I, I_Q)$  denote variance of estimators of  $var(I_I), var(I_Q)$  and  $cov(I_I, I_Q)$ , respectively.

The error of the estimation of phase profile is determined from the variance of  $\varphi_k$ . The anti-trigonometric function is expanded in the neighborhood of  $\varphi_k$  according to the Taylor's theorem [32]:

$$\varphi_k = \arctan(\bar{R}) + \arctan'(\bar{R})(R - \bar{R}) + L_2(R) \quad (11)$$

$L_2(R)$  represents for the Lagrange remainder term.  $\varphi_k$  Can be approximated by (8) if we ignore the remainder term.

$$\varphi_k \approx \arctan(\bar{R}) + \arctan'(\bar{R})(R - \bar{R}) \quad (12)$$

the variance of  $\varphi_k$  can be analyzed with:

$$D(R) \approx \arctan'(\bar{R})D(R) \quad (13)$$

substitute formula (9) into Eq. (12), the following expression for the variance of phase noise can be obtained:

$$D(\varphi_k) = \frac{\bar{R}^2}{(1 + \bar{R}^2)^2} \left( \frac{\sigma_I^2}{I_I^2} + \frac{\sigma_Q^2}{I_Q^2} \right) = \frac{\sigma^2/2}{1 + g^2} \quad (14)$$

## Funding

National Natural Science Foundation of China (NSFC) (61525502, 61435006); National High Technology 863 Research and Development Program of China (No. 2015AA015502); Projects 1-YW0S, 4-BCBH of the Hong Kong Polytechnic University (PolyU) 5208/13E of the Hong Kong RGC (PolyU) 1-ZVFL.